Concentration Effects in Aqueous NaCl Solutions. A Molecular Dynamics Simulation

ARTICLE *in* THE JOURNAL OF PHYSICAL CHEMISTRY · OCTOBER 1996

Impact Factor: 2.78 · DOI: 10.1021/jp961317h

2 AUTHORS, INCLUDING:

Alexander P Lyubartsev
Stockholm University
155 PUBLICATIONS **4,739** CITATIONS

SEE PROFILE

Concentration Effects in Aqueous NaCl Solutions. A Molecular Dynamics Simulation

Alexander P. Lyubartsev* and Aatto Laaksonen†

Division of Physical Chemistry, Arrhenius Laboratory, Stockholm University, 106 91 Stockholm, Sweden

Received: May 8, 1996; In Final Form: July 8, 1996[⊗]

A series of constant-temperature/constant-pressure molecular dynamics simulations of aqueous NaCl solutions at different salt concentrations is carried out to investigate the structure and the dynamical properties. The simulations were performed with the number of molecules ranging from 256 to 2000. The simulations cover several nanoseconds to ensure the convergence of the results and to enable a proper determination of ion−ion radial distribution functions. The flexible SPC water model is used as the solvent, while the ions are treated as charged Lennard-Jones particles. Only a weak influence of the salt concentration is found on the ion−ion pair correlation functions. The structures of the hydrated shells around ion pairs are studied using three-body correlation functions. The self-diffusion and interdiffusion coefficients are found to decrease with an increase of salt concentration. Molar conductivities are calculated at different salt concentrations. The residence times of water molecules in the hydration shells as well as the residence times of contact and solvent-separated ion configurations are determined.

1. Introduction

Computer simulations of aqueous ionic solutions have received much attention due to their importance in many areas of physical chemistry and molecular biophysics.[1,2] Studies of the structure of the hydrated shells around the ions,[3−7] calculations of the ion−water radial distribution functions,[5−10] energetics and thermodynamics of ion−water interactions,[11−14] and calculations of the potential of mean force at infinite dilutions[4,15−20] have been reported in the literature. Most of these studies are done by simulating a single ion or an ion pair in water solution.

Despite their importance, ionic solutions at finite concentrations, *i.e.*, when at least several ion pairs are present, are considerably less studied using computer simulations. One of the key issues in studies of concentrated ionic solutions is the ion−ion correlation, which can be described using radial distribution functions (RDFs). The interionic RDFs are related to the potential of mean force (PMF) of ions[19] and to the effective interaction potential of ions in solution.[21] A knowledge of realistic PMFs or effective ion−ion potentials becomes particularly important in simulation studies of large biomolecular and other polyelectrolyte systems, where an explicit account of solvent molecules is still too expensive and one has to use simplified models with an effective account of the solvent.

The reported RDF[21−24] or PMF[15−20] results appear to be quite often in contradiction to each other and show an apparent dependence on the used model. A general picture arises in several works: the anion−cation potential of mean force has usually two minima, first corresponding to the contact ion pairs (CIP configuration) and the second corresponding to the solvent-separated ion pairs (SSIP configuration). However, the intensities, *i.e.*, the relative importance of these minima, vary largely from work to work. For example, the first minimum of the NaCl PMF is reported between −2 kJ/M (ref 17) and −20 kJ/M (ref 15). Correspondingly, the first maximum of the Na−Cl RDF varies considerably in different works.[21−26] These differences can be explained partially by the different models used for water and the ions. Another problem is that the determination of the potential of mean force requires expensive free-energy simulations. While in the calculations of the radial distribution functions, one is faced with poor statistics because of the low ratio of the number of ions to the total number of molecules and the low (comparatevely to the typical simulation time) mobility of the ions. A final difficulty is the necessity of an accurate treatment of the long-range electrostatic interactions[15] in systems where the Debye radius typically has the order of the box length.

Under these circumstances, it is important to carry out an extended analysis of the existing ionic solution models and to try to take into account all possible sources of artifacts and weaknesses. It is necessary to investigate the effects of the limited simulation time, use of the finite cutoff radii in force calculations, and evaluate the details and performance of the molecular dynamics algorithms, to mention a few. In this paper, we present a rather extensive molecular dynamics study of aqueous NaCl solutions. We have performed a series of sufficiently long (several nanoseconds) simulations at different salt concentrations, ranging from 0.5 to 4 M. The molecular and potential models and details of molecular dynamical algorithm are described in section 2. In section 3, we present results on ion−ion radial distribution functions, including an analysis of statistical errors, as well as the effects of simulation time and the system size. We have also analyzed the structures of the hydrated shells around ions and ion pairs using three-body correlation functions.

In addition to the hydration structure and interionic correlations, the dynamical behavior of the ions in solution and the waters hydrating the ions are of central importance. Molecular dynamics simulations can give a direct insight into the molecular motion, which can be helpful for understanding and interpretation of results obtained from NMR studies, conductivity measurements, and other experimental techniques. For more information about the experimental work, the reader is referred to the review by Ohtaki and Radnai.[2] A variety of dynamical properties of ionic solutions have been studied using molecular dynamics simulations.[27−30] The information about the behavior of hydrated water molecules and the hydrated ions themselves is still rather limited and fragmented.[2] In section 4, we present

* Also affiliated with Scientific Research Institute of Physics, St. Petersburg State University, 198904, St. Petersburg, Russia. E-mail: sasha@tom.fos.su.se.

† E-mail: aatto@tom.fos.su.se.

⊗ Abstract published in *Advance ACS Abstracts,* September 1, 1996.

S0022-3654(96)01317-2 CCC: $12.00

TABLE 1: Potential Parameters

atom	q_i	σ_i, Å	ϵ_i, kJ/M
O	−0.82	3.1656	0.65
H	0.41	0	0
Na^+	1	2.35	0.544
Cl^-	−1	4.4	0.419

the results of time autocorrelation functions, self-diffusion and interdiffusion coefficients, residence times, and their concentration dependences. Finally, the conclusions are summarized in section 5.

2. Models and Methods

There exist a large number of water and water−ion interaction models in the literature, from simple dipole hard sphere[31] or Stockmayer liquid[32] to interaction potentials, obtained from *ab initio* quantum mechanical calculations.[33] The more realistic the used potential model is, the more computer time is required for the simulations. In this work, we have used a standard type of force field, in which all the intermolecular interactions are expressed as a sum of the electrostatic and the Lennard-Jones potentials with parameters fitted for each atomic type. This type of force field is rather simple and allows us to make the computations fast. Nevertheless, these potentials have shown to give a realistic description of intermolecular interactions provided that the interaction parameters are properly fitted. We have chosen the flexible SPC water model[34] and the Smith−Dang parameters for ion−water and ion−ion interactions.[8,27] The atom−atom potentials are expressed as

$$\psi(r_i,r_j) = \frac{q_i q_j}{r_{ij}} + 4\epsilon_{ij}\left[\left(\frac{\sigma_{ij}}{r_{ij}}\right)^{12} - \left(\frac{\sigma_{ij}}{r_{ij}}\right)^{6}\right] \qquad (1)$$

where off-diagonal Lennard-Jones parameters σ_{ij} and ϵ_{ij} are given using the combination rules[35]

$$\sigma_{ij} = (\sigma_i + \sigma_j)/2$$

$$\epsilon_{ij} = \sqrt{\epsilon_i \epsilon_j}$$

The potential parameters q_i, σ_i, and ϵ_i are given in Table 1. The parameters for the ions are determined in ref 8 by fitting them to gas-phase binding enthalpy data for small sodium and chlorine ion−water clusters. This fitting was done for the SPC/E water model. In our work, we used the flexible SPC model, which has almost the same parameters and structural properties as the SPC/E model. The flexible SPC model contains some polarization effects due to its flexibility. The diffusion coefficient and the dielectric constant of the flexible SPC model are very close to the experimental values.[36] These features of this particular water model should be important for studies of ionic solution with strong electrostatic interactions.

We used a constant-temperature/constant-pressure molecular dynamics algorithm[37] in our MD simulations. The Nose−Hoover thermostat parameters were set to 30 fs for the thermal bath and 700 fs for the volume fluctuations. In all our simulations, the temperature was 300 K and the pressure was 1 atm. Other characteristic simulation parameters are given in Table 2. The simulations were performed at four different salt concentrations. In addition, two of these (0.55 and 0.9 M) were made with different box sizes to evaluate possible size effects. A separate 200-ps simulation was made for 256 water molecules without ions to have reference data for the bulk water.

All the simulations were carried out in a cubic box with periodic boundary conditions, using mininum image convention. The Ewald method was applied for treatment of long-range electrostatic interactions.[38] The cutoff radius in the reciprocal space, k_{max}, was determined from the condition that the exponent factor in the k-space term $\exp(-\pi^2 k_{max}^2/(L\alpha)^2) = \exp(-8.5)$ and the screening parameter α was taken as $\alpha = 2.8/R_{cut}$. Under these conditions, the cutoff distance in the real space (R_{cut}) can be optimized for a maximum computation speed (evidently, a decrease of R_{cut} reduces the computation time for the real space term, while it increases the computation time for the reciprocal space term). In our largest simulation with 2000 molecules, we have used $R_{cut} = 14$ Å, while in other cases, the cutoff distance was set equal to a half of the box length.

TABLE 2: Simulation Parameters

	run						
	0	1	2	3	4	5	6
no. of H_2O	256	490	1960	248	484	236	220
no. of ion pairs	0	5	20	4	8	10	18
salt concn, M	0	0.55	0.55	0.87	0.9	2.2	4.1
av box length, Å	19.75	24.5	38.7	19.76	24.4	19.44	19.35
simulation time,[a] ns	0.2	2.5	1.5	3.5	2	3	3

[a] After 200 ps of equilibration.

In the starting configuration, the molecules were located with random orientations on the FCC lattice, the ions being distributed randomly in the volume. Then the system was equilibrated during 200 ps. We have used the double time step algorithm by Tuckerman et al.,[39] with a small time step of 0.2 fs for intramolecular and short-range (less than 4.5 Å) intermolecular interactions and a large time step of 2 fs for the other interactions. Our test simulation in the constant-energy ensemble clearly showed that time steps larger than 0.2/2.0 fs led rapidly to a poor energy conservation and to a noticeble shift in the calculated pressure. The calculations were carried out on an IMB SP2 at the center of parallel computing (PDC), the Royal Institute of Technology, Stockholm.

3. Static Properties

3.1. Thermodynamical Properties. The results for the densities of NaCl solutions at different concentrations are given in Table 3 together with the experimental densities of the NaCl solutions. There is a small difference (0.01 g/cm^3) between the experimental and the calculated densities which is constant throughout the concentration interval. This may be a consequence that the original flexible SPC model has somewhat higher density compared to the experimental one. Our simulations of pure water show that the density of the flexible SPC water is 1.006 g/cm^3. This is in agreement with the *NVT* simulations by Wallqvist and Teleman,[40] who found that at experimental density, this model gives a negative pressure.

The different contributions into total energy are also presented in Table 3. One can see that water−water interaction energy $E(H_2O-H_2O)$ is increasing (becomes less negative) with an increase of the salt concentration. This effect takes place mainly due to the disruption of the hydrogen bonds. The ion−water interactions ($E(Na^+ - H_2O)$ and $E(Cl^- - H_2O)$) both become weaker upon an increase of the salt concentration, because of the influence of other ions on the hydrated shell. An interesting observation is that the total interaction energy of an ion with other molecules is less sensitive to the salt concentration. The increase of the ion−water energy becomes compensated by the decrease of the ion−ion energy. The same holds for water molecules (see the term "$E(H_2O$ with others)" in Table 3), for which the weakening of the hydrogen bonds is compensated by a larger contribution from ion−water interactions.

The total solvation energy can be determined as the energy for the process of transferring the solute molecules from the

TABLE 3: Some Thermodynamical and Structural Properties of Aqueous NaCl Solutions[a]

	run							
	0	1	2	3	4	5	6	stat error
salt concn, M	0	0.55	0.55	0.87	0.9	2.2	4.1	
density								
calcd, g/cm^3	1.006	1.028	1.029	1.043	1.044	1.085	1.151	0.002
exptl,[36] g/cm^3	0.997	1.02	1.02	1.033	1.034	1.076	1.14	
E_{tot}/N_{tot}	−41.9	−49.1	−49.2	−53.4	−53.7	−69.0	−91.3	0.1
different contributions to the total energy								
$E(H_2O-H_2O)/N_{H_2O}$[b]	−41.9	−35.9	−36.1	−33.1	−32.6	−25.5	−13.4	0.2
$E(Na^+ - H_2O)/N_{Na}$	−745[c]	−675	−670	−590	−568	−443	−375	10
$E(Cl^- - H_2O)/N_{Cl}$	−575[c]	−564	−561	−518	−505	−387	−340	15
E(ion−ion)/N_{Na}		−155	−163	−205	−223	−348	−404	15
$E(H_2O$ with others)[d]	−97.8	−98	−99.5	−100	−99	−99.5	−101	1
$E(Na^+$ with others)[d]		−778	−780	−778	−785	−772	−773	10
$E(Cl^-$ with others)[d]		−725	−730	−738	−752	−745	−755	15
$E_{solv}/N_{ion\ pairs}$	−775[e]	−807	−813	−820	−824	−802	−790	10
coordination numbers								
Na^+		5.78	5.8	5.5	5.6	5.42	5.3	0.05
Cl^-		6.9	6.9	6.8	6.8	6.9	7.1	0.05
NaCl CIP config per ion		0.044	0.041	0.09	0.096	0.30	0.49	
NaCl SSIP config per ion		0.37	0.42	0.52	0.57	1.2	2.2	
NaNa SSIP config per ion		0.06	0.07	0.14	0.12	0.4	0.63	
ClCl SSIP config per ion		0.18	0.16	0.22	0.25	0.8	1.7	

[a] All the energies are given in kJ/M. For more details, see the text. [b] Including the intramolecular bond energy. [c] Result of ref 41 for a single ion in SPC/E water. [d] Interaction energy of a selected molecule with all other molecules. [e] Result of ref 27 for a separated ion pair, the same ion model, and SPC/E water model.

TABLE 4: Some Results of Simulation Run 3, Obtained from Averaging over 0.5-ns Intervals of the MD Trajectory

	averaging time, ns								
	0.2−0.7	0.7−1.2	1.2−1.7	1.7−2.2	2.2−2.7	2.7−3.2	3.2−3.7	av	stat error[a]
first max NaCl RDF	8.2	4.8	3.2	0.6	3.	8.9	6.2	5.0	1.1
second max NaCl RDF	2.0	2.6	3.5	2.3	2.2	1.6	2.5	2.4	0.2
first max NaNa RDF	2.8	1.2	2.6	1.0	0.2	0.7	1.3	1.4	0.4
first max ClCl RDF	1.2	1.1	0.6	1.5	1.3	1.7	0.7	1.15	0.15
$E(Na_+ - H_2O)/N_{Na}$, kJ/M	−615	−548	−623	−625	−613	−568	−552	−592	11
$E(Cl^- - H_2O)/N_{Cl}$, kJ/M	−434	−468	−522	−578	−543	−529	−523	−514	17

[a] Calculated as the corresponding variance, divided by $N^{1/2}$.

ideal gas phase into the solvent, and it is equal to the difference of the total energy of the solution and energy of the same amount of bulk water. These values are listed in Table 3. The solvation energy at infinite dilution is taken from ref 27, which was calculated for a separated (more than 6 Å) Na−Cl ion pair using the same ion model as in our work but a rigid SPC/E water model. One can see a nonmonotonous dependence on the salt concentration, with a weak minimum at a concentration of about 1 M. This means that it is energetically more profitable to install ion pairs in solution at this concentration. It is quite remarkable that the experimental dependence of NaCl activity coefficients[42] also shows a minimum at this concentration. The connection here is not direct: the activity coefficients are related to the free energy and its concentration dependence. At the same time, the internal energy gives a major contribution to the free energy.

3.2. Structural Pair Correlations. The structure of liquids and solutions can be conveniently studied using radial distribution functions. Calculations of radial distribution functions are usually a straightforward task in molecular dynamics simulations. The water/water and water−ion correlation functions, calculated in our simulations, are in perfect agreement with corresponding results from other simulations.[5−10] The hydration numbers, obtained by integrating the first minimum of ion−oxygen RDF, are presented in Table 3. It can be observed that the Na^+ hydration number is steadily decreasing with an increase of the salt concentration. This is most likely because some water molecules in the hydration shell are occasionally substituted by chlorine ions. This effect does not take place for the chlorine hydration numbers. A sodium ion, forming a contact ion pair with a chlorine ion, does not substitute a water molecule in the hydration shell around chlorine. Rather, it installs itself there. As a result of this, the size of the Cl^- hydration shell increases slightly with the salt concentration.

Obtaining the ion−ion RDFs is a matter of much more effort than calculations of the ion−water RDF. In fact, we have found that a reliable evaluation of the ion−ion RDFs requires a simulation time of several nanoseconds. The main reason for the extended simulations is the small number of ions in the simulation cell, resulting in poor statistics. In addition, a slow ion diffusion leads to a slow sampling of the configurational space. Thus, the characteristic time which is required for a considerable change of ion configuration has the order of hundred picoseconds. In Table 4, we present some results obtained from averaging over several sequential 500-ps pieces of the simulations. The first observation is that the results for the first maximum of NaCl RDF are unstable, varying more than 1 order of magnitude. The reason for this behavior is that the CIP and SSIP configurations are separated by a high (several kT) effective potential barrier and transitions between them are rare events (a detailed analysis of the corresponding residence time will be given in the next section). The ion−water interaction energies also fluctuate strongly, which leads to relatively high statistical errors for these energies. Moreover, some correlation between the water−ion interaction energies and the value of the first maximum of NaCl RDF can be seen from Table 4. A low value of this maximum corresponds to low values of ion−water energies. The ions in this case are almost fully hydrated and do not come into direct contact with

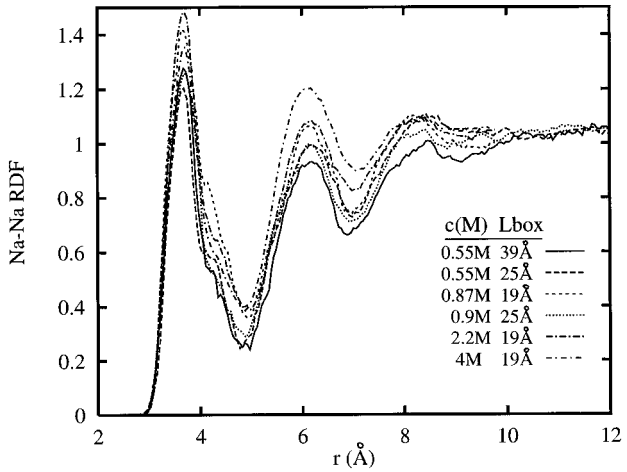

Figure 1. Na−Na radial distribution functions.

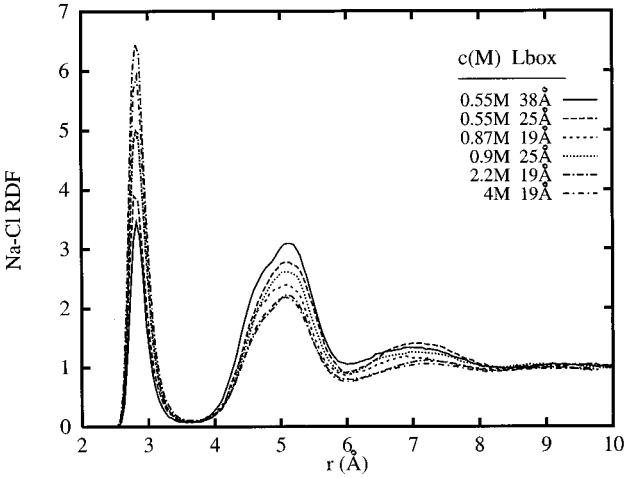

Figure 2. Na−Cl radial distribution functions.

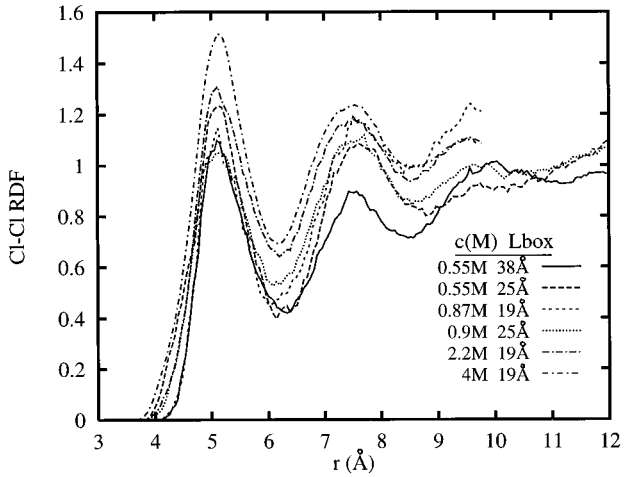

Figure 3. Cl−Cl radial distribution functions.

each other. On the contrary, an occasional formation of contact ion pairs leads to weaker ion−water interactions.

The case with the lowest salt concentration, presented in Table 4, is worst from the statistical point. The other simulations contain more ion pairs, giving better sampling statistics even after a shorter simulation time. Still, we may consider a simulation time of the order of 1 ns as a minimum requirement for a reliable evaluation of ion−ion RDF.

The resulting ion−ion RDFs are presented in Figures 1−3. The typical features of these RDFs correspond to the results obtained previously in other simulations[21−25] and to the potential of mean force calculations.[15−19] The NaCl RDFs have a first contact maximum at 2.8 Å, second solvent-separated maximum at 5.1 Å, and a weak third maximum at about 7 Å corresponding to an attraction of fully hydrated ions. The RDFs between the like-charged ions also have several maxima. The RDFs show a rather weak dependence on salt concentration. The most noticeable effects of the increase of the salt concentration are an increase of the first maximum and decrease of the second and third maxima of the NaCl RDF. The RDFs for like-charged ions tend to increase with increasing the salt concentration.

Having obtained the ion−ion RDFs, we can determine how many ions occur in the contact or in the solvent-separated configurations. This can be done by integrating the corresponding maximum of ion−ion RDF in the same way as one calculates the hydration numbers:

$$x = c\int_{r_1}^{r_2}\rho(r)\,4\pi r^2\,\mathrm{d}r \qquad (2)$$

Relative populations of CIP and SSIP states are important quantities in the theory of ionic association[43] and can be measured using infrared and Raman spectroscopy.[44] The values calculated in our work are listed in Table 3. One can see that in 0.5 M solution, only about 4% of the ions form ion pairs, whereas at 4 M concentration, about half of the ions are in contact with opposite ions.

Differences in RDFs, obtained at the same concentration but varying the system size, are generally small. One can note that the second maximum of the NaCl RDF is higher for larger systems; however, the difference is of the same order as the statistical error. Also, some differences are observed at large distances close to the half box length, which most likely take place due to boundary effects.

3.3. Three-Body Correlation Functions. The radial distribution functions do not give a full description of the structural properties. In general, an average spatial assembly of more than two particles cannot be uniquely characterized from pair correlation functions. Additional information can be obtained from third- and higher-order correlation functions.

Calculations of higher-order correlation functions are a straightforward task in computer simulations; they are calculated in the same manner as the RDFs. The three-body distribution function $\rho_3(r_1,r_2,r_3)$ for a spacially and orientationally homogeneous system is a function of three variables, for example, the three distances between the three particles. It is, however, rather difficult to display this function of three variables in a two-dimensional figure. To simplify the task, one may fix one of the variables, say, the distance between the first and the second particle r_{12}, and build a contour map of the function of the two remaining variables. This function is proportional to the density distribution of the third particle in the vicinity of fixed first and second particles:

$$\rho(r_3|r_{12}=\text{const}) = \rho_3(r_1,r_2,r_3)/\rho_2(r_{12})$$

where $\rho_2(r_{12})$ is the RDF between the first and the second particles. The distance r_{12} can be taken to correspond to a maximum of RDF between these two particles. In this case, the maxima of the $\rho(r_3|r_{12}=\text{const})$ function show typical configurations for the three particles. In three-dimensional space, this function has an axial symmetry with respect to the line connecting the first and the second particles.

Examples of three-body distribution functions are shown in Figures 4−7.[45] They were taken from run 4, corresponding to 0.9 M concentration. In Figure 4, contour maps of oxygen distribution (solid lines) and hydrogen distribution (dashed lines)

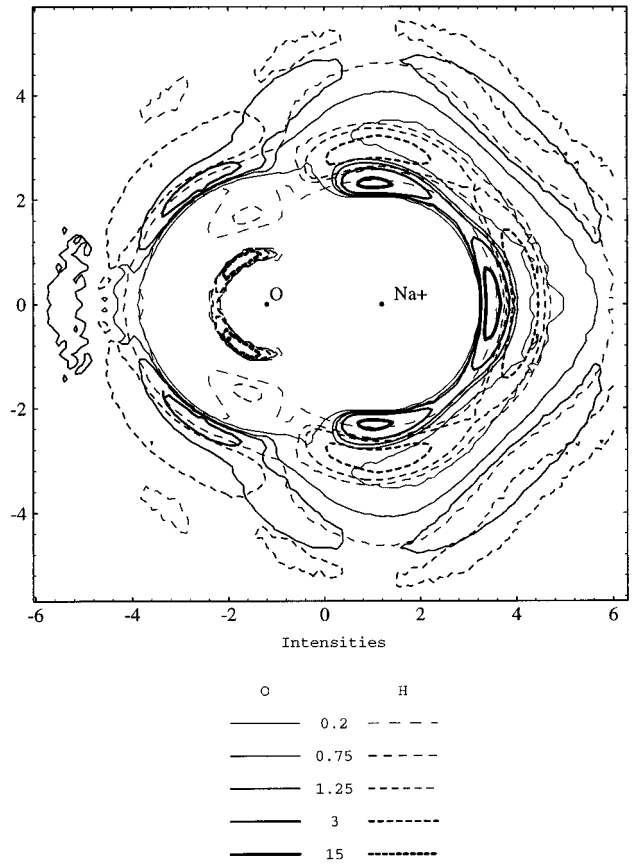

Figure 4. Contour map of oxygen (solid lines) and hydrogen (dashed lines) densities around Na^+ and O atoms fixed at 2.35 Å.

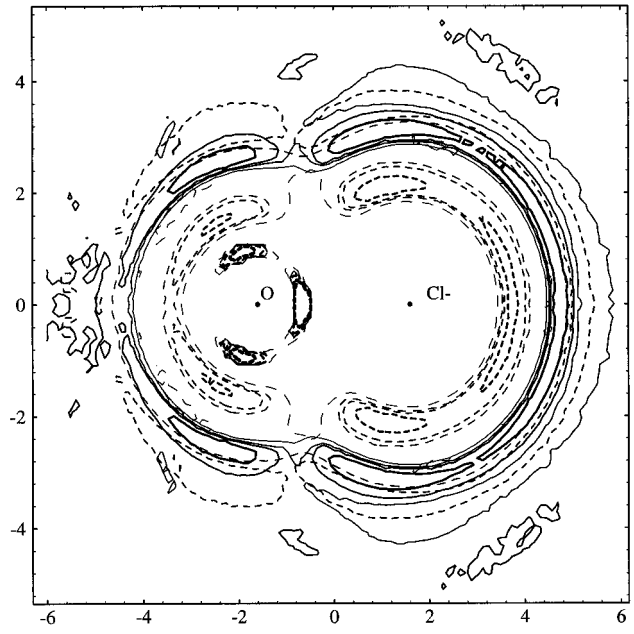

Figure 5. Contour map of oxygen (solid lines) and hydrogen (dashed lines) densities around Cl^- and O atoms fixed at 3.21 Å.

around Na and O atoms separated on 2.35 Å are displayed. Positions of oxygen atoms in the first hydration shell are well-defined; they are located in three perpendicular directions from the sodium ion and yield hydration number 6. The second hydration shell clearly shows an octahedral shape.

The structure of the chlorine hydration shell (oxygen and hydrogen distributions around the Cl−O pair) is shown in Figure 5. There is no such well-defined symmetry as can be seen in the case of the sodium ion. Positions of the two water molecules

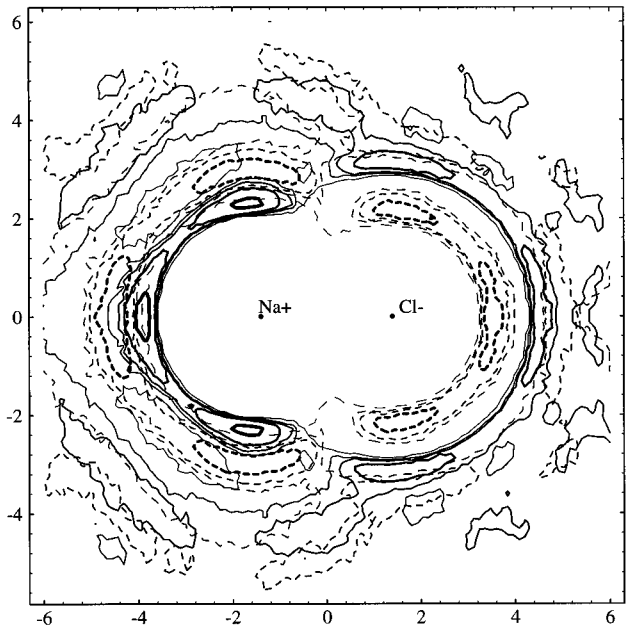

Figure 6. Contour map of oxygen (solid lines) and hydrogen (dashed lines) densities around Na^+ and Cl^- ions fixed at 2.81 Å.

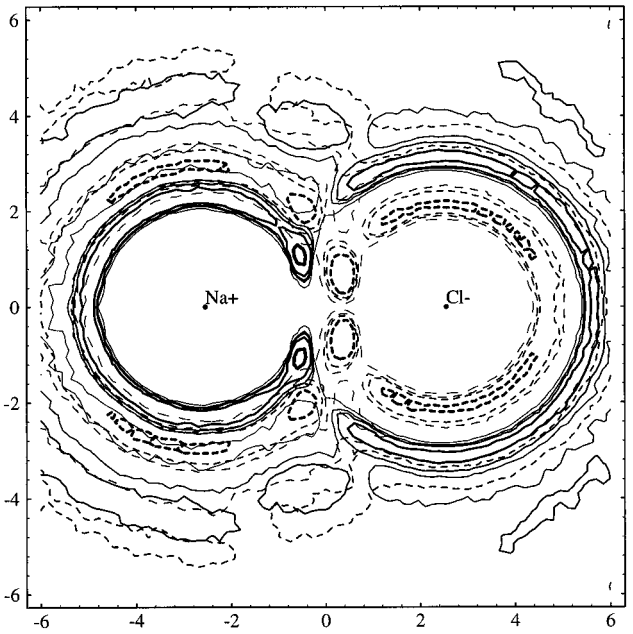

Figure 7. Contour map of oxygen (solid lines) and hydrogen (dashed lines) densities around Na^+ and Cl^- ions fixed at 5.1 Å.

in the hydration shell are hardly correlated, with the exception that they cannot come too close to each other. There is no noticeable second hydration shell around the chlorine ion.

The structure of the hydration shell around the contact ion pair is shown in Figure 6. It can be seen that the hydration shell of the ion pair repeats typical features of the pure sodium and chlorine shells (Figures 4 and 5). It looks like one of the ions is entering into the hydration shell of the other ion instead of one of the water molecules. It does not seem to change the rest of the hydration shell noticably.

The distributions of oxygen and hydrogen around the solvent-separated ion pair are shown in Figure 7. The positions and the orientations of the water molecule linking the two ions are well-defined. This water molecule is not found on the line between the sodium and the chlorine ions. Rather, it seems to orient itself with respect to each of the ions in the same fashion as was found in the hydration shell of an isolated ion (compare

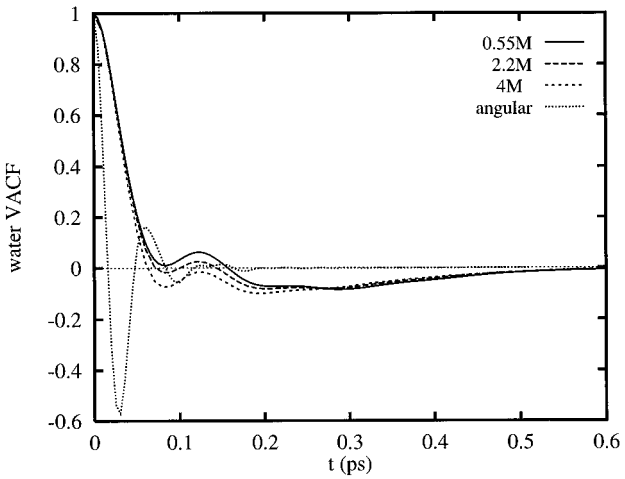

Figure 8. Translational and angular velocity autocorrelation functions of water molecules in the ionic solution.

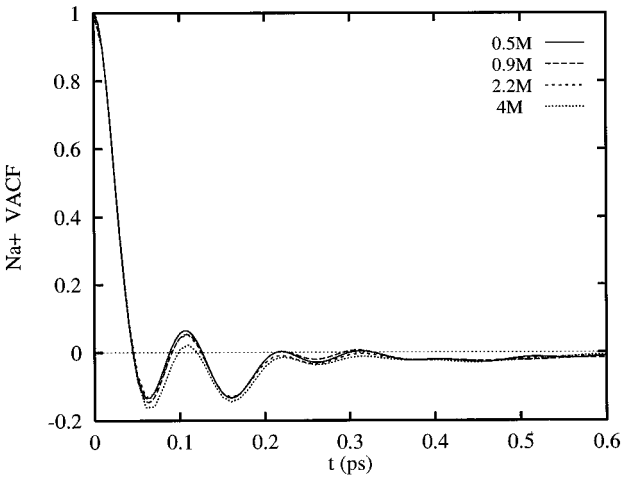

Figure 9. Velocity autocorrelation functions of Na^+ ion at different concentrations.

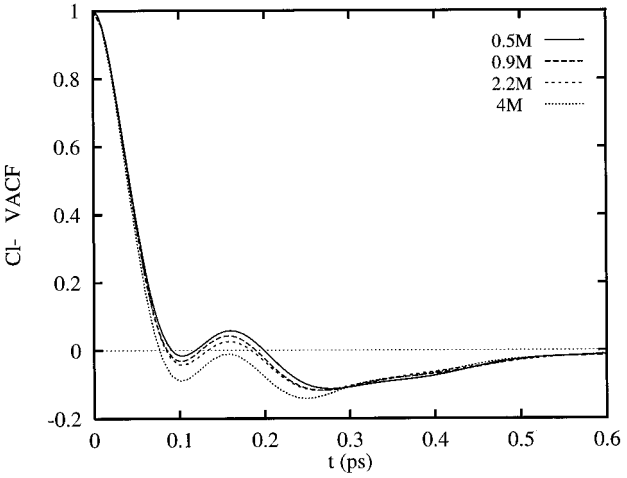

Figure 10. Velocity autocorrelation functions of Cl^- ion at different concentrations.

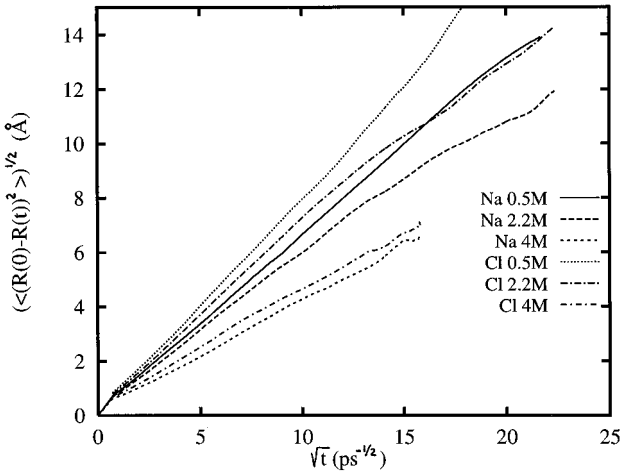

Figure 11. Average displacement of an ion at different salt concentrations.

Figures 4 and 5). The positions of other oxygens in the sodium hydration shell are somewhat diffuse with respect to the chlorine ion.

4. Dynamical Properties

4.1. Velocity Autocorrelation Functions. The normalized velocity autocorrelation function (VACF) is defined as

$$f_v(t) = \frac{\langle v_i(t_0 + t) v_i(t_0) \rangle_{i,t_0}}{\langle v_i(t_0)^2 \rangle_{i,t_0}} \tag{3}$$

where the average is taken over both particle number i and time t_0. The calculated VACF for the water molecules and the ions at different salt concentrations are shown in Figures 8−10. VACFs appear to have a rather weak dependence on the salt concentration. An increase of the salt concentration leads to some strengthening of the negative part of VACF, most noticeable on the time scale of 0.1−0.3 ps. This means a greater probability for a particle to turn back after this time and, hence, an enhancement of the oscillations in the microscopic dynamics of the molecules and slowing down of the diffusion.

Analogously with eq 3, the normalized angular velocity autocorrelation functions can be defined as

$$f_w(t) = \frac{\langle w_i(t_0 + t) w_i(t_0) \rangle_{i,t_0}}{\langle w_i(t_0)^2 \rangle_{i,t_0}} \tag{4}$$

The angular VACF for water molecules is also displayed in Figure 8. It decays much faster than the translational VACF. No noticeable dependence of $f_w(t)$ on the salt concentration was found.

4.2. Self-Diffusion. The translational self-diffusion coefficients can be determined by two methods: from mean square displacement

$$D = \lim_{t \to \infty} \frac{\langle [R(t) - R(0)]^2 \rangle}{6t} \tag{5}$$

or from the velocity autocorrelation functions

$$D = \frac{kT}{m} \int_0^\infty f_v(t)\, dt \tag{6}$$

We have used both methods to determine D. While calculating the diffusion coefficients from mean square displacement, we have taken the slope of the curve in eq 5 at time t between 50 and 200 ps. In fact, the convergence within a 5% interval was already reached after about 10 ps. Attempts to calculate the mean square displacement on a longer time scale lead to a growing uncertainty due to a worsening of sampling statistics when time t becomes comparative with the simulation time. The mean square displacements of ions are displayed in Figure 11. One can see that during 0.5 ns, the ions on average travel a distance of 10−15 Å, which is less than the box size and

TABLE 5: Diffusion Coefficients (in 10^5 cm^2/s)

	run							
	expt[a]	0	1	2	3	4	5	6
salt concn, M	0	0	0.55	0.55	0.87	0.9	2.2	4.1
(a) Calculated from Velocity Autocorrelation Functions								
H_2O	2.35	2.25	2.05	2.09	1.75	1.72	1.54	1.05
Na^+	1.33		0.95	0.97	0.76	0.69	0.62	0.43
Cl^-	2.03		1.24	1.28	1.03	1.06	0.89	0.53
(b) Calculated from mean square displacements								
H_2O		2.12	2.01			1.66	1.49	0.97
Na^+			0.88		0.69	0.70	0.63	0.42
Cl^-			1.28		1.04	0.98	0.89	0.55
H_2O, expt[47]	2.35				2.17		2.0	1.7

[a] Experimental results for infinite dilution.[42]

comparative (especially for low salt concentrations) to the average distance between the ions. This is the main reason why we need such a long time to calculate ion−ion distribution functions.

The final results for the self-diffusion coefficients are presented in Table 5. All the diffusion coefficients, both for water and for ions, decrease with an increase of the salt concentration, as expected; an especially noticable fall of the diffusion coefficients takes place at high salt concentrations. There exists other simulation data of self-diffusion coefficients of ions, calculated at infinite dilution (a single ion in the cell). Lee and Rasaiah[41] obtained for the same model of ions and SPC/E water $D_{Na^+} = 1.2 \times 10^{-5}$ cm^2/s and $D_{Cl} = 1.7 \times 10^{-5}$ cm^2/s. Guardia *et al.*[17] obtained for the Pettitt−Rossky ion model and flexible SPC water $D_{NA^+} = 1.1 \times 10^{-5}$ cm^2/s and $D_{Cl^-} = 2.5 \times 10^{--5}$ cm^2/s. Simulations of the Na^+ ion in TIP4P water yield sufficiently lower diffusion coefficients: $D_{NA^+} = 0.74 \times 10^{-5}$ cm^2/s in ref 29 and $D_{Na^+} = 0.67 \times 10^{-5}$ cm^2/s in ref 46. For the Cl^- ion in TIP4P water, the self-diffusion coefficient was obtained in ref 28 as $D_{Cl^-} = 1.57 \times 10^{-5}$ cm^2/s. It has also been observed that the way the long-range electrostatic forces are treated strongly affects the calculated diffusion coefficients.[28,40]

The self-diffusion coefficient for bulk water was obtained as $D_v = 2.2 \times 10^{-5}$ cm^2/s (run 0). This result is lower than previous estimations for the flexible SPC model ($D_v = 2.54 \times 10^{-5}$ cm^2/s in ref 36 and $D_v = 3.1 \times 10^{-5}$ cm^2/s in ref 40), but it is closer to the experimental diffusion coefficient of water 2.35×10^{-5} cm^2/s.[42] As well as our results, experimental data[47] also show an decrease of the diffusion coefficient of water with an increase of the salt concentration, although this effect is more pronounced in our simulation.

4.3. Interdiffusion. The interdiffusion coefficient D_{12} is determined from the time integration of the normalized current correlation function $J(t)$:[48]

$$D_{12} = kT\frac{m_1 + m_2}{2m_1m_2}\int_0^\infty J(t)\,\mathrm{d}t \tag{7}$$

$$J(t) = \frac{\langle j(t)j(0)\rangle}{\langle |j(0)|^2\rangle} \tag{8}$$

where

$$j(t) = \sum_{i=1}^{N} q_i v_i(t) \tag{9}$$

is a microscopic estimator of the current flow. If the ions move independently from each other, the interdiffusion coefficient is equal to the mean value of their self-diffusion coefficients. Ion−ion association and correlations in the ion motion lead to a deviation between the interdiffusion coefficient and the mean self-diffusion coefficient, which is described by the parameter Δ:[30]

$$D_{12} = (1 - \Delta)(D_1 + D_2)/2 \tag{10}$$

The interdiffusion coefficient is also related to the equivalent (or molar) conductivity of the ionic solution:

$$\Lambda = \frac{2N_A e^2}{kT} D_{12}$$

Calculated values of the interdiffusion coefficients and equivalent conductivities, together with the corresponding experimental values, are given in Table 6. The calculated conductivities are systematically somewhat less than the experimental ones.[49] This is a consequence of the overall slower diffusion in the chosen potential model comparing with the experimental data (see Table 5). Still, the calculated and experimental conductivities have the same trend, and the difference between them is nearly constant throughout the concentration range.

TABLE 6: Interdiffusion Coefficients (D_{12}) and Molar Conductivities (Λ)

	concn, M			
	0.55	0.9	2.2	4.1
D_{12}, 10^5 cm^2/s	1.10	0.84	0.67	0.47
Δ[a]	0.03	0.05	0.08	0.02
Λ_{calc}, 10^{-4} m^2 S mol^{-1}	83	63	52	38
Λ_{exp}(ref 49)[b]	92	76	63	49

[a] Mean values of self-diffusion coefficients calculated from VACF were used. [b] At $T = 291$ K.

The interdiffusion coefficients are somewhat lower than the average of the self-diffusion coefficients. This is a consequence of ionic association. Opposite charged ions in an ion pair tend to move together, making a negative contribution from nondiagonal terms in eq 8 into the current correlation function. This effect more or less disappears at very high concentrations ($\Delta = 0.02$ for 4 M solution), because most of the ions have several (accounting solvent-separated) neighbors and no isolated ion pairs exist.

To directly observe correlations in the motion of ions, we calculated the following function. Let two ions occur on distance R_0 at moment $t = 0$ with their coordinates $r_1(0)$ and $r_2(0)$. We will follow their motion and calculate the scalar product of their displacements, averaging over all such pairs:

$$\rho(R_0,t) = \langle (r_1(t) - r_1(0))(r_2(t) - r_2(0))\rangle|_{|r_1(0)-r_2(0)|=R_0} \tag{11}$$

If two ions form a stable ion pair and move together, this function would be proportional to time t (as the mean square displacement of a single particle). If the motion of the ions is by no means correlated (for example, at very large R_0), this function is equal to zero. In other cases, we can expect an intermediate behavior.

We have calculated the function $\rho(R_0,t)$ for (Na^+, Cl^-) pairs at two values of R_0 corresponding to a contact ($R_0 = 2.81$ Å) and to a solvent-separated ($R_0 = 5.1$ Å) ion pair. The results are shown in Figures 12 and 13. For a contact ion pair at 0.5 M concentration, the slope of the function $\rho(R_0,t)$ is almost the same as for the self-diffusion of the Na^+ ion (Figure 4). For higher concentrations, the correlations become weaker in ion motion. These are also several times weaker for solvent-

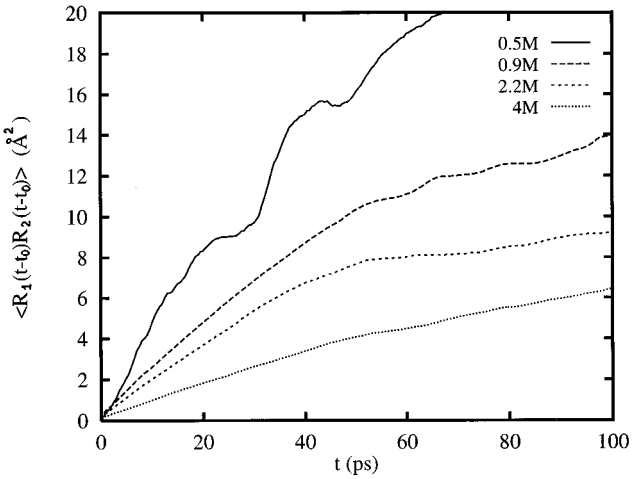

Figure 12. Displacement correlation function $\rho(R_0,t)$ for Na^+Cl^- contact pair ($R_0 = 2.81$ Å; see eq 11).

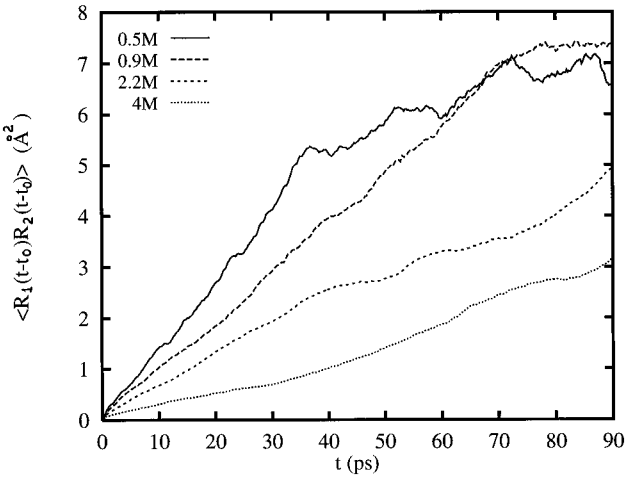

Figure 13. Displacement correlation function $\rho(R_0,t)$ for Na^+Cl^- solvent-separated pair ($R_0 = 5.1$ Å; see eq 11).

separated ion pairs (see Figure 10) and almost disappear for ions separated more than 7 Å from each other.

4.4. Residence Time. How long water molecules stay in the hydration shell around different ions at different physical conditions is important for understanding the dynamics of the hydrated water molecules.[2] For example, it is related to the "dynamic hydration number", which provides an estimate of the number of water molecules which are bound to an ion on a time scale in which the coordinated shell of a bulk water molecule is renewed.[33]

We define a border of the hydration shell r_{hyd} as the first minimum of ion−oxygen RDF. Then, according to ref 33, we define the function $P_j(t,t_i;t^*)$, which takes the value 1 if molecule j lies within the first coordination shell of the ion at both time steps t_i and $t_i + t$ and in the interim does not leave the coordinates shell for any continuous period, longer than t^*. Otherwise, it takes the value 0. The parameter t^* is introduced to ignore cases when a molecule leaves the coordinated shell only temporarily and returns back without properly entering the bulk solution. As in other works,[27,33] we set $t^* = 2$ ps.

Then we define the function

$$p(t) = \langle P_j(t,t_i;t^*)\rangle_{i,j}/\langle P_j(0,t_i;t^*)\rangle_{i,j} \qquad (12)$$

which gives a probability for a molecule in the hydrated shell to remain there during time t. These functions are shown in Figure 14. After a fast initial fall, they decay almost exponentially: $p(t) \sim \exp(-t/t_s)$, where t_s is the residence time.

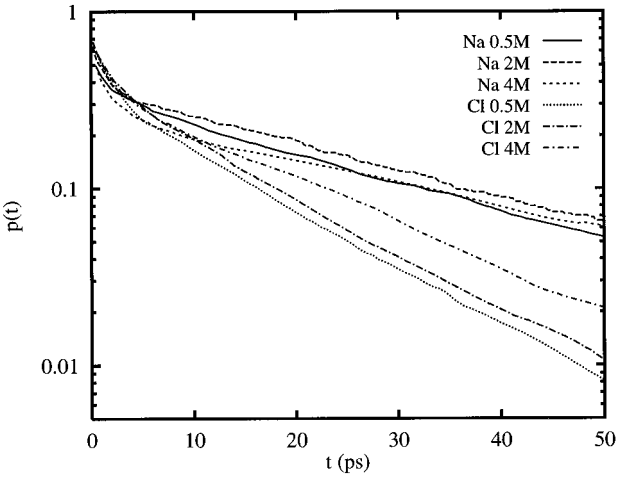

Figure 14. Probability $p(t)$ (see eq 12) for a water molecule in the coordinated shell of an ion to stay there after time t.

TABLE 7: Residence Times (in ps)

	concn, M				
	0.55	0.9	2.2	4.1	stat. error
H_2O-H_2O	4.7	4.9	5.4	6.5	0.1
H_2O-Na	21	20.5	22	22	0.5
H_2O-Cl	10.4	11	11.7	13.	0.5
NaCl, CIP	40 ± 15	50 ± 5	46	44	2
NaCl, SSIP	18	20	19.5	21	1

The results obtained for the residence time at different concentrations are listed in Table 7. An interesting observation is that while the residence time for Cl^- increases with an increase of the salt concentration, it preserves generally the same value for Na^+. The increase of the residence time for Cl^- ions may take place due to contribution from the ion pairs in which Cl^- and Na^+ ions share some of the water molecules with longer residence times.

The residence time for two water molecules, found in contact, is also increasing with increasing salt concentration. This may be because more and more water molecules become involved in the hydration of the ions and this will increase the average residence time for the waters. The residence times of water molecules in the hydration shells of ions are estimated in other works at infinite dilution. The result in ref 41 is 26 ps for Na^+ and 9.0 ps for Cl^-, and the result in ref 27 is 29 ps for Na^+ and 12 ps for Cl^-. These results were obtained for the SPC/E water model and are similar to our results. For the MCY water model, Impey *et al.*[33] obtained much lower results: 10 ps for Na^+ and 4.5 ps for Cl^-.

In analogue to the residence time of water molecules, we can define the residence time of contact and solvent-separated configurations of the ions. Because of the poor statistics of these events, we could not draw function $p(t)$ properly to determine the decay parameter. Instead, we have used an average of time intervals during which the ions were in CIP or SSIP configurations, respectively. Observe that for a purely exponential decay, these two definitions are equivalent. The results are shown in Table 7. The residence time for both CIP and SSIP configurations does not seem to depend on the salt concentration, at least in the limits of statistical error. Contact configurations are more stable than solvent-separated one. The average time for CIP configurations is about 50 ps, but we have registered several cases when a NaCl contact pair existed a time longer than 200 ps. The long-living CIP configurations were one of the obstacles for reliable RDF calculations, especially when only a few ion pairs are present in the simulation box (runs 1 and 3 in Table 1, for example). While a CIP

configuration exists, it gives a strong contribution to the first maximum of the ion−ion RDF. Thereafter, a long period may follow, up to several hundred picoseconds, without any CIP configurations at all. This may also cause some instability in the calculations of other properties.

5. Conclusions

We have carried out a series of molecular dynamics simulations of a model NaCl ionic solution at different concentrations and also varying the system size. The great benefit of computer simulation is the possibility to directly observe every molecular detail of the model system. Of course, the obtained information is relevant only to the extent of how the interaction potentials are able to mimic the real system. The potentials employed in this work were derived mostly empirically by fitting to some experimental thermodynamical and structural data,[8] and the results previously reported on this model were in line with other theoretical and experimental studies of NaCl ionic solutions.

An advantage of carrying out a series of simulations varying a parameter (e.g., concentration) is that such studies reveal some dependences and trends which are usually much less sensitive to the model in use than some specific quantities. Our studies of the structural and dynamical aspects of the hydrated shell of ions, ion association vs salt concentration, may contribute to a deeper understanding of microscopic processes in solutions.

We have also checked the possible influence of the system size on the simulation results. Simulations carried out for different system sizes but at the same ion concentrations yielded mostly the same results, and existing deviations were in the limits of statistical error. This may be considered to be a confirmation that long-range electrostatic interactions were properly taken into account using the Ewald method.

Acknowledgment. This work was supported by the Swedish Natural Science Foundation (NFR) and by the Wenner−Gren Foundation. We are thankful to the Center for Parallel Computing (PDC) at the Royal Institute of Technology for granting the computer facilities.

References and Notes

(1) Heinzinger, K. *Phys.* **1985**, *131B*, 196.
(2) Ohtaki, H.; Radnai, T. *Chem. Rev.* **1993**, *93*, 1157.
(3) Bounds, D. G. *Mol. Phys.* **1985**, *54*, 1335.
(4) Pettitt, B. M.; Rossky, P. J. *J. Chem. Phys.* **1986**, *84*, 5836.
(5) Belch, A. C.; Berkowitz, M.; McCammon, J. A. *J. Am. Chem. Soc.* **1986**, *108*, 1755.
(6) Degreve, L.; Quintale, C., Jr. *Chem. Phys. Lett.* **1993**, *208*, 530.
(7) Parera, L.; Berkowitz, M. L. *J. Chem. Phys.* **1994**, *100*, 3085.
(8) Dang, L. X.; Smith, D. E. *J. Chem. Phys.* **1993**, *99*, 6950.
(9) Hummer, G.; Soumpasis, D. M.; Neumann, N. *Mol. Phys.* **1992**, *77*, 769.
(10) Migliore, M.; Forlini, S. L.; Spohr, E.; Palinkas, G.; Heinzinger, K. *Z. Naturforsch.* **1986**, *41*, 826.
(11) Chandrasekhar, J.; Spellmeyer, D. C.; Jorgensen, W. L. *J. Am. Chem. Soc.* **1984**, *106*, 903.
(12) Lybrand, T. P.; Chosh, I.; McCammon, J. A. *J. Am. Chem. Soc.* **1985**, *107*, 7793.
(13) Jayaram, B.; Beveridge, D. L. *J. Phys. Chem.* **1990**, *94*, 7288.
(14) Gowda, B. T.; Benson, S. W. *J. Chem. Phys.* **1983**, *79*, 1235.
(15) Smith, D. E.; Haymet, A. D. J. *Fluid Phase Equilib.* **1993**, *88*, 79.
(16) Dang, L. X.; Pettitt, B. M.; Rossky, P. J. *J. Chem. Phys.* **1992**, *96*, 4046.
(17) Guardia, E.; Rey, R.; Padro, J. A. *J. Chem. Phys.* **1991**, *95*, 2823.
(18) Friedman, R. A.; Mezei, M. *J. Chem. Phys.* **1995**, *102*, 419.
(19) Pratt, L. R.; Hummer, G.; Garcia, A. E. *Biophys. Chem.* **1994**, *51*, 147.
(20) Karim, O. A.; McCammon, J. A. *J. Am. Chem. Soc.* **1986**, *108*, 1762.
(21) Lyubartsev, A. P.; Laaksonen, A. *Phys. Rev. E* **1995**, *52*, 3730.
(22) Hummer, G.; Soumpasis, D. M.; Neumann, M. *J. Phys.: Condens. Matter* **1994**, *6*, A141.
(23) Hummer, G.; Soumpasis, D. M.; Neumann, M. *Mol. Phys.* **1993**, *81*, 1155.
(24) Zhu, S. B.; Robinson, G. W. *J. Chem. Phys.* **1992**, *97*, 4336.
(25) Chialvo, A. A.; Cummings, P. T.; Cochran, H. D.; Simonson, J. M.; Mesmer, R. E. *J. Chem. Phys.* **1995**, *103*, 9379.
(26) Llano-Restrepo, M.; Chapman, W. G. *J. Chem. Phys.* **1994**, *100*, 8321.
(27) Smith, D. E.; Dang, L. X. *J. Chem. Phys.* **1994**, *100*, 3757.
(28) Perera, L.; Essmann, U.; Berkowitz, M. L. *J. Chem. Phys.* **1995**, *102*, 450.
(29) Lee, S. H.; Rasaiah, J. C. *J. Chem. Phys.* **1994**, *101*, 6964.
(30) Payne, V. A.; Forsyth, M.; Ratner, M. A.; Shriver, D. F.; de Leeuw, S. W. *J. Chem. Phys.* **1994**, *100*, 5201.
(31) Patey, G. N.; Valleau, J. P. *J. Chem. Phys.* **1975**, *63*, 2334.
(32) Patey, G. N.; Carnie, S. L. *J. Chem. Phys.* **1983**, *78*, 5183.
(33) Impey, R. W.; Madden, P. A.; McDonald, I. R. *J. Chem. Phys.* **1983**, *87*, 5071.
(34) Toukan, K.; Rahman, A. *Phys. Rev. B* **1985**, *31*, 2643.
(35) Hansen, J. P.; McDonald, I. R. *Theory of Simple Liquids*; Academic: London, 1976.
(36) Anderson, J.; Ullo, J. J.; Yip, S. *J. Chem. Phys.* **1987**, *87*, 1726.
(37) Melchionna, S.; Coccotti, G.; Holian, B. L. *Mol. Phys.* **1993**, *78*, 533.
(38) Allen, M. P.; Tildesley, D. J. *Computer Simulation of Liquids*; Clarendon: Oxford, 1987.
(39) Tuckerman, M.; Berne, B. J.; Martyna, G. J. *J. Chem. Phys.* **1992**, *97*, 1990.
(40) Wallqvist, A.; Teleman, O. *Mol. Phys.* **1991**, *74*, 515.
(41) Lee, S. H.; Rasaiah, J. C. *J. Phys. Chem.* **1996**, *100*, 1420.
(42) *CRC Handbook of Chemistry and Physics*; Lide, D. R., Ed.; CRC: Boca Raton, FL, 1994.
(43) Winstein, S.; Clippinger, E.; Fainberg, A. H.; Robinson, G. C. *J. Am. Chem. Soc.* **1954**, *76*, 2597.
(44) *Advances in Infrared and Raman Spectroscopy*; Clark, R. J., Hester, R. E., Eds.; Heyden: London, 1976.
(45) Color density maps of these and some other three-body correlation functions are available on the author's WWW site: *http://www.fos.su.se/physical/sasha/shells/hydro.html.*
(46) Berkowitz, M.; Wan, W. *J. Chem. Phys.* **1987**, *86*, 376.
(47) Muller, K. J.; Hertz, H. G. *J. Phys. Chem.* **1996**, *100*, 1256.
(48) J. P. Hansen, J. P.; Joly, F.; McDonald, I. R. *Phys. A* **1985**, *132*, 472.
(49) *Lange's Handbook of Chemistry*; Dean, J. A., Ed.; McGraw-Hill: New York, 1985.

JP961317H